



An analytical approach for modelling unmanned aerial vehicles and base station interaction for disaster recovery scenarios

Eugene Casmin^{1,2} · Enver Ever³

Accepted: 20 March 2024 / Published online: 18 April 2024
© The Author(s) 2024

Abstract

Unmanned Aerial Vehicles (UAVs) are an emerging technology with the potential to be used in various sectors for various applications and services. In wireless networking, UAVs can be used as a vital part of the supplementary infrastructure to improve coverage, principally during public safety emergencies. Because of their affordability and potential for widespread deployment, there has been a growing interest in exploring the ways in which UAVs can enhance the services offered to isolated ground devices. Large areas may lose cellular coverage following a public safety emergency that impacts critical communication infrastructure. This prompts the need for the employment of D2D communication frameworks as a complement. In such critical conditions, timely response and network connectivity are essential factors for reliable communication. This study focuses on the mathematical models of UAV-based wireless communication in the context of disaster recovery. Particularly, we aim to model a queuing framework comprising UAVs as mobile relay nodes between the stranded user devices and neighbouring operational base stations. We present an iterative solution with a novel method for generating initial conditions for the two-stage queuing model. The approximate approach presented is validated for its accuracy using discrete-event simulation. The effects of various factors on performance measures are also analysed in detail. The validation results show that the discrepancy between the analytical approach and the simulation is less than 5%, which is the confidence interval of the simulation.

Keywords UAV relay nodes · Disaster recovery environment · Two-stage open queuing networks · Iterative queuing solution · Discrete-event simulation

Eugene Casmin and Enver Ever have contributed equally to this work.

✉ Enver Ever
eever@metu.edu.tr

Eugene Casmin
e.owilla@campus.fct.unl.pt

¹ Departamento de Engenharia Electrotécnica, Faculdade de Ciência e Tecnologia, FCT, Universidade Nova de Lisboa, 2829-516 Caparica, Portugal

² IT, Instituto de Telecomunicações, Aveiro, Portugal

³ Computer Engineering, Middle East Technical University Northern Cyprus Campus, 99738 Guzelyurt, Mersin 10, Turkey

1 Introduction

Uninterrupted coverage is a vital aspect of disaster recovery communication infrastructure, due to the dynamic nature of factors affecting both stranded individuals and search and rescue teams. Hence, the need for continuous network coverage strategies becomes evident. This can be achieved through on-ground devices [1] and UAVs [2]. Focusing on UAVs, their mobility enhances resource management and provides greater control to search and rescue authorities.

Public safety emergencies, whether man-made (e.g., terror attacks) or natural (e.g., earthquakes), can lead to the compromise of wireless network base stations due to physical damage or power outages. Current UAV frameworks for addressing network needs may face criticism for resource optimisation or being dependent on continuous ground device operation for effectiveness. These challenges significantly hinder search and rescue operations, where speed and precision are critical. Such operations require targeted

information about individuals in the disaster recovery area. In this context, a streamlined infrastructure framework with minimal overhead is essential.

Mobile devices are well-suited for tracking the movement and location of stranded individuals in inactive cells. Connecting these devices to operational base stations in neighbouring cells can be achieved through various means. Therefore, both academia and industry have investigated strategies to develop practical solutions, with recent research highlighting the use of UAVs to overcome these challenges.

In [3], UAV networks for disaster management are discussed, along with open research issues. The optimization of UAV flight paths for device-to-device (D2D) communication in disaster scenarios to meet energy constraints is presented in [4]. The study in [5] explores relaying with multiple UAVs involving multi-hop and dual-hop links, as well as the determination of optimal hovering positions. It's important to note that these schemes primarily focus on stationary or hovering UAVs acting as substitute base stations and relay nodes. In [5], two typical multi-UAV relaying schemes involving a single multi-hop link and multiple dual-hop links are also examined, with a focus on deriving optimal hovering positions.

One popular UAV-assisted method of alleviating wireless networking needs in a disaster recovery situation is employing UAVs as substitute base stations. In this case, the UAV hovers above the stranded cell and provides cellular coverage for data and voice packets to the mobile devices on the ground. In such scenarios, the UAV deployed is not mobile, and the concept does not provide for incorporating the mobility-related factors into the models presented. An integrated approach utilising both UAVs and ground cluster heads is explored in [2]. The study delves into two main scenarios. The first scenario employs a single stationary UAV within a stranded cell, which links to an emergency communication vehicle located at a distance. This is facilitated by multiple UAV relay nodes positioned between the source (the stationary UAV in the stranded cell) and the destination (the emergency communication vehicle). It's important to note that neighbouring cells have fully operational base stations in this scenario, which aligns with our study's focus on localized disaster areas. The second scenario involves ground clusters communicating with a selected cluster head, which then communicates with a stationary UAV hovering above the stranded cell. The hovering UAV, in turn, connects to one or more relay nodes (other UAVs) positioned between it and an emergency communication vehicle outside the disaster recovery area. This vehicle acts as a mobile makeshift base station, bridging the gap between the stranded cell and operational stations beyond the disaster area. In this case, multiple stationary UAVs are used as relay nodes due to their immobility. These scenarios provide a relevant context

for our study, particularly the first scenario that deals with neighbouring operational base stations.

There has been extensive research into using UAV-assisted frameworks for various practical applications, including disaster recovery, as seen in [6]. Recently there has been a particular focus on framework modelling, i.e., defining the optimum conditions for which UAV-assisted network enhancement can be applied as well as designing UAVs for use in disaster recovery [2, 7–9]. We have encountered research on various general aspects of queuing analysis in UAV-assisted communications. For instance, in [10], a queuing analysis approach is presented for multi-hop networks. Such an approach could be instrumental in modelling queues for ad-hoc scenarios such as Flying Ad-Hoc Networks (FANETs). All these form a firm foundation for our goal to add to work that includes mobile UAV relay nodes and implements an iterative method of solving for queuing performance measures in the context of disaster recovery.

The analytical models presented in this study provide an accurate approach for queuing analysis, allowing the inclusion of the required devices and heterogeneous network links in the communication chain. Additionally, the presented analytical solution is computationally more efficient compared to simulation-based evaluations. The contributions of this study can be summarised as follows:

- The operational approach of the fully mobile UAV-RNs, focused on the efficient provision of uninterrupted wireless service for isolated mobile devices with the support of surviving ground base stations (BSs), is examined.
- A two-stage open queuing model is introduced, incorporating relaying and feedback mechanisms for D2D communication within the UAV-assisted wireless network improvement framework during disaster recovery.
- To mitigate the well-known state explosion problem which is common for the elementary solutions based on systems of simultaneous equations [1, 11], an iterative solution method for the two-stage open queuing networks [12] is further improved for the specific scenarios considered.
- An augmented approach is introduced to generate the initial conditions required to kick off the iterative method.
- The iterative method results are presented comparatively in terms of accuracy and efficacy with the results obtained by discrete event simulation for validation. The results presented have less than 5% discrepancy, which is within the confidence interval of the simulation program, and the iterative approach is significantly more efficient in terms of computation time.

2 Related work

Recently, surveys [6, 13] have highlighted various wireless communication scenarios where UAVs can enhance network throughput, particularly as hovering BSs. They address issues like network performance, service stability, physical layer considerations (e.g., non-line-of-sight communications analysis), and the sustainability of UAV-based networking in comparison to more traditional solutions.

In all of these discussions, the prevailing sentiment is that the benefits of UAV-based solutions, including their flexibility, on-demand deployment, high mobility, and energy efficiency [13], outweigh the drawbacks like limited battery power, no-fly zone restrictions, and safety concerns. In essence, the advantages justify the effort needed to mitigate the disadvantages.

In the context of this study's subject matter, it's essential to mention existing research on UAV-based or UAV-assisted disaster recovery management for public safety networks (PSNs). Table 1 displays the studies considering the performance evaluation of these systems. The table supports our claim that the majority of existing research focuses on framework modelling and addressing physical challenges in the deployment of UAV-based disaster recovery networks. Our aim in this study is to enhance this field by contributing to explicit queuing analysis for UAV-assisted frameworks within this context.

In studies considering UAVs as mobile relay nodes, such as [6], UAVs are used as mobile pure relay nodes

in Wireless Sensory Networks (WSNs). They collect data from WSNs in the field and transmit it to a central data collection point. This approach replaces traditional static relay nodes, which led to problems like packet loss and single points of failure due to a multi-hop topology. Another example, [8] involves UAVs serving as mobile pure relay nodes in dynamic environments. These UAV relay nodes facilitate communications within a Vehicular Ad-Hoc Network (VANET) by collecting data packets from source nodes (typically vehicles) and delivering them to sink nodes (the destination vehicles). This back-and-forth operation helps the VANET overcome challenges associated with the rapid mobility of nodes.

UAVs adopting a “dump-truck” approach selectively utilize transmission energy only when within range of the source/destination [22], thus consuming less energy compared to static relay nodes acting as substitute BS, which require continuous transmission energy during their entire hovering time. Furthermore, flexibility is evident in the ability to adjust infrastructure configuration to cater to the specific needs of the scenario, including coverage area, UAV velocity, and transmission rates.

Another relevant study involving UAVs in wireless networking applications is [7], where Fenyu Jiang and Chris Philips investigate improving the throughput of UAVs deployed in disaster recovery scenarios, akin to our case. They establish a connection between UAV-RN bandwidth, throughput, and UAV trajectory to enhance network performance. The study results in a UAV-RN trajectory planning scheme employing the Dual-Sampling method for

Table 1 Performance evaluation methods used in literature

Studies	Evaluation method	Contribution
[14]	USARSim simulation environment	A post-disaster solution for an emergency communications system established by UAVs
[15]	Custom simulation	An analysis of the advantages gained by harnessing the mobility of UAVs for disaster scenarios
[16]	Physical deployment/experimentation	A solution using unmanned aerial vehicles (UAVs as data mules or routers) to mitigate issues caused by sensor network faults in monitoring natural disasters
[17]	Better Approach To Mobile Ad-hoc Networks (BATMAN) discovery & routing protocol	Addressing challenges to enhance the reliability and performance of collaborative autonomous aircraft in aerial sensing during disaster recovery
[18]	Python software simulation and physical demo using quadrotor UAVs	A novel approach for handling a large-scale autonomous deployment of a UAV communications network for disaster recovery
[19]	Opportunistic Network Environment (ONE) simulator testbed	Proposes a model for a FANET scenario assisted by Delay Tolerant Networks (DTN). The analytical perspective focuses on addressing challenges in communication and data exchange among UAV nodes for sparse FANETs
[20]	3D environment rendering	Addressing mobility management and coverage lifespan through a distributed mobility algorithm based on the virtual spring model
[21]	Modelling and custom simulation	A dynamic framework empowering ground users to autonomously allocate transmission power in either UAV-based or MBS-based communication is presented

maximising data transmission throughput, bandwidth scheduling and contention schemes. This article provides a valuable reference for our proposed model's framework parameters. It's worth noting that while the paper delves deeply into the mathematical aspects of the framework, including bandwidth scheduling and trajectory planning, it lacks a queuing analysis of the UAV-based relaying solution. Therefore, our study offers crucial insights to fill this gap.

The framework presented in [1] serves as an example, for modelling similar interactions. It involves using mobile cluster heads as relay nodes (RNs) to extend coverage to stranded user devices during disaster recovery. The ground relay nodes are devices within the operational base station's coverage area, providing signals to devices outside the base station's coverage. These relay nodes may be chosen randomly from devices on the edge of the operational cell or through an intelligent selection algorithm. Any device at the operational cell border, termed a "Relay UE" (Relay User Equipment), could potentially serve as a ground relay node. However, this approach introduces another problem: inconsistent signal strength when the current ground relay node's battery power depletes. This inconsistency can hinder search and rescue operations, particularly if emergency packet transmissions in the disaster area experience unpredictable delays. These issues form the basis of our proposed model and will henceforth be referred to as the comparative model.

The queuing system used in [1] is a Markov model. The first queuing stage is for packets received from the stranded mobile devices by the relay node. Hence the stage is referred to as the "uplink stage". In the second stage, the received packets are subsequently forwarded to the operational BS in whose area of coverage the RN is. This stage is hence referred to as the "relay stage". It is also important to note that the queuing model takes into account packet loss probability (denoted by $1 - \theta_1$) between the uplink and relay stages as well as the feedback probability (denoted by θ_2). The framework proposed aims to provide continuous cell signal for voice and data communications to stranded devices in the disaster area. The iterative solution presented is successfully applied to a 3D Markov process with good levels of accuracy and proved to be computationally light in comparison to the solution based on a system of simultaneous equations explored for the same scenario.

In [11], a scheme aimed at improving network speed by introducing a 5 G femtocell in a 4 G macrocell is investigated. The resulting framework also calls for the use of a two-stage tandem queuing model. Unlike in [1] the proposed tandem queuing model employed in this paper constitutes tandem Markov queues i.e., an M/M/c/L queue followed by an M/M/1/L queue. An analytical solution based on a system of simultaneous equations is improved upon by introducing a

product-form solution and an accompanying custom simulation to evaluate the proposed framework.

To this point, we have presented the building blocks of the work tendered by our own study. It can therefore be gleaned from this that there is room for improvement in the research available regarding explicit analysis of workable solutions presented for the use of UAVs as RNs in disaster recovery, in terms of the queuing and consequent efficient analytical solution.

3 System model

In this section, the role of the UAVs as relay nodes deployed in the disaster area is explained, and the queuing model is presented with the subsequent derivations and solutions based on a system of simultaneous equations.

3.1 The proposed framework

Consistent with the comparative case study in [1], the precise placement of the relay node within the disaster area is critical. The ideal location ensures equal signal strength for both packet transmission up-link and relay stages. Furthermore, the UAV relay's touted rapid mobility is achieved by circulating the stranded cell at an optimal speed, maintaining area coverage without compromising packet delivery.

While we adopt the conical area coverage concept from [9], we maintain the traditional hexagonal cell shape common in wireless networks. This choice allows us to plan for a specific number of neighbouring cells in our proposed framework. Furthermore, as suggested in [23], we recommend implementing this framework using fixed-wing UAVs rather than rotary ones, as the former offer advantages such as smaller size, lower energy consumption for variable altitudes, higher speed, greater payload capacity, and longer flight durations.

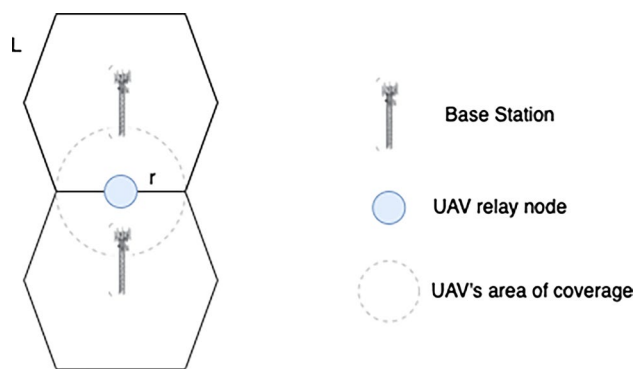
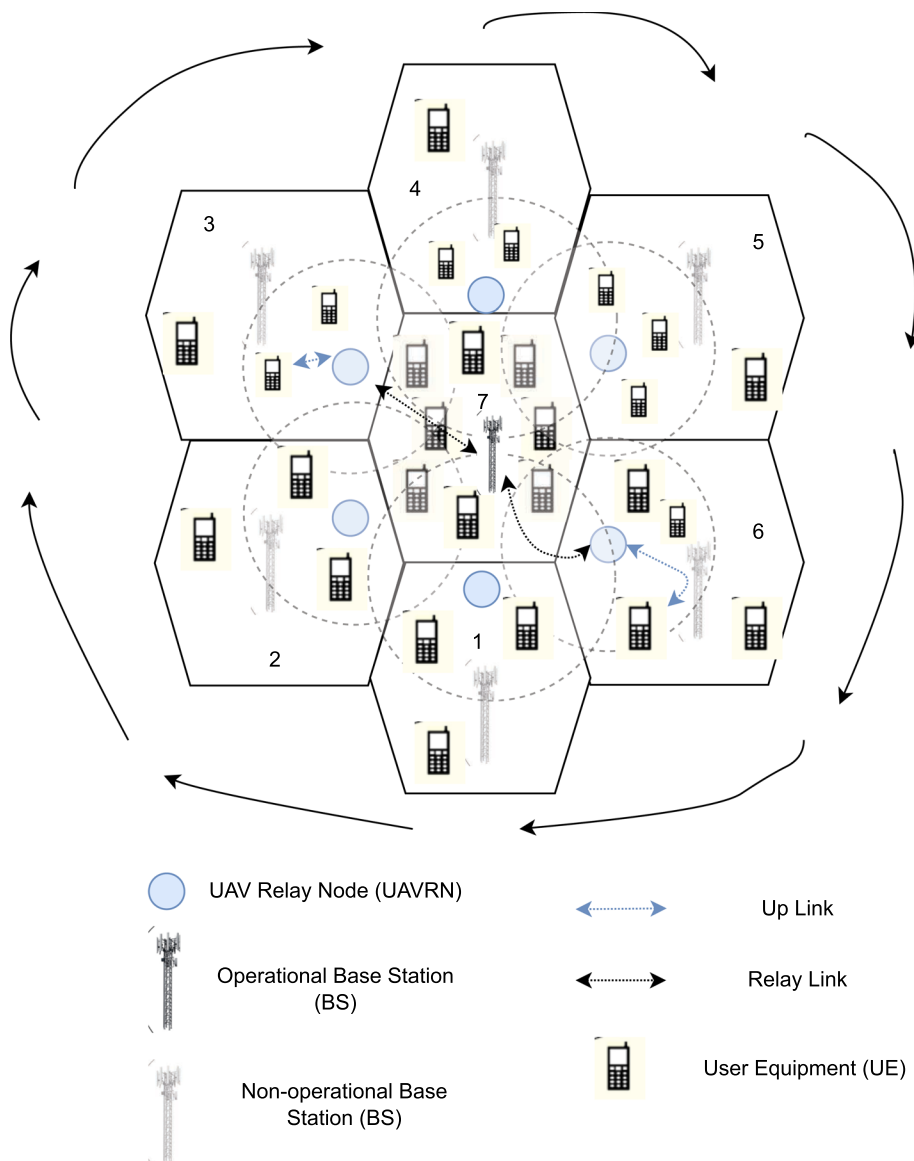


Fig. 1 Ideal UAVRN placement in the proposed framework

Fig. 2 Proposed framework with highly mobile UAV-RN



In Fig. 1, the optimal UAV relay node placement is illustrated at the border of two cells. This position is considered ideal because it ensures continuous coverage for as many ground UEs as possible in the stranded cell while remaining within the operational base station’s coverage area. Figure 2 below depicts the operational approach of the proposed framework when considering these factors.

In Fig. 2, the middle cell (Cell 7) has an operational BS, whereas all the BSs in the neighbouring cells (Cells 1 to 6) have sustained damage and are not operational. The UAV-RN navigates the boundaries of Cell 7, extending its coverage to the stranded cells and relaying SOS packets to the emergency channel of the operational BS in Cell 7. The mobile UAVs are employed in a similar manner to the studies presented in [6, 8], and [24]. The UAV flies in a trajectory along the periphery of the region of interest with

a speed that allows relaying the packets. Search and rescue authorities use this data to locate device holders in the disaster area. This process is repeated to support search and rescue operations. This configuration aims to provide relay service to as many UEs as possible. The UEs can send their SOS packets while they are within the coverage area of the UAV-RN, which circulates in proximity (within the range of the operational Base Station) to the operational cell. In the event that a UE moves to a region that the UAV-RN can cover during its navigation, it can send the SOS packets when the UAV-RN visits that particular region. Please note that the configuration for different cellular setups may vary, and the generated traffic can easily be adapted to be covered as the mean arrival rate to the UAV-RN. It is critical to study the interaction between the UAV-RN and the operative BS

in order to make sure that both of them are able to cope with the traffic generated.

Considering the realism of the framework and the viability of a mathematical model, the following assumptions are present for the modelling attempt:

1. This framework does not cater to voice and data transmission for stranded cell devices. Instead, it employs compact emergency SOS packets, which introduce far less traffic for transmission by both devices and the UAV-RN. These SOS packets contain the device's serial number (16 bytes), GPS coordinates (6 bytes), and timestamp (date and time in hours, minutes, & seconds, 13 bytes). This totals approximately 35 bytes per packet, in stark contrast to the average data packet size of 1000 to 1500 bytes as per [25].
2. The stranded devices have SOS capabilities: This feature already exists for most, if not all, current smart devices. At the very least, as per 5 G (seeing as this is one of the target network infrastructures for this framework, we are able to use its device density estimates) research [26], it is expected that there will be at least one smart device with SOS capabilities in every square metre (10^6 devices per square kilometre). This maintains the high probability that a stranded individual is within a reasonable distance from a device that is broadcasting SOS packets in the event that some devices are rendered physically unable to broadcast the SOS packet.
3. At least one neighbouring cell must have an operational base station, as depicted in Fig. 2, for the framework to maintain continuous coverage.
4. For the variable altitude path, the proposed implementation in [9] is employed, which allows us to control the number of devices within the area of coverage by varying the altitude of the UAV relay node during its flight.
5. The ground device broadcasting scheme is not such that the devices are synchronised to broadcast the SOS packets simultaneously. Instead, it is arbitrary. To this effect, the primary arrival rate at the UAV-RN stage, λ_1 , is essentially predicated on the assumption that per unit of time, a number of devices within the range of the UAV-RN's area of coverage are broadcasting their respective SOS packets.
6. The UAV-RN receiving channel is always listening for a connection with the stranded devices on the ground. Upon establishment of connection, the packets are received as long as they are being broadcast.
7. The stranded devices are uniformly distributed throughout the cell.
8. The packet handling scheme at the Base Station endpoint is intelligent enough to eliminate duplicate SOS

packets received due to originating packets (those within the coverage area of the operational base station) being in the area of coverage of the UAV-RN. As mentioned in assumption 1, the SOS packets are labelled with a field containing the serial number of the device from which the packet originated. This information (for the originating devices in the cell with the operational BS) is part of the routing information present at the BS; hence, the BS is able to eliminate duplicate packets delivered by the UAV-RN. In an unlikely case where a small fraction of duplicate messages occur at BS, the relatively small SOS packets are not expected to overwhelm the BS.

9. The operational base stations in the disaster area transmit a feedback packet acknowledging receipt of the UAV-RN's payload. This is a vital part of the queuing model.
10. Co-tier interference is known to arise among network elements that belong to the same tier within the network. In the proposed framework, co-tier interference in D2D communication that the SOS packet broadcasts may cause is assumed to be handled by the communication standard. The co-tier interference incurred at a D2D receiver from a neighbouring D2D transmitter can be mitigated through proper user pairing and frequency assignment techniques [27]. Power control, beam forming, or spectrum slicing methods can also be used to manage the possible interference [28]. Furthermore, some studies also use approaches such as Stackelberg game formulation, where the UE pays the price as an incentive to the BS, causing energy trading and interference pricing [29]. Considering all these approaches, the queuing model of the system should be able to accommodate various rates of incoming traffic to UAV-RN.

3.2 Queuing model

This study presents an analytical model to investigate the queuing performance of the proposed framework, discussed at length in the preceding subsection. When the UAV is within range of both the stranded devices on the ground and an operational base station, a queuing model can be used for the SOS packets received from the stranded devices and relayed to the operational BS. Simultaneously, the operational base station will be servicing the devices in its own coverage area. Additionally, we visualise the base station responding to the UAV relay node with a feedback packet acknowledging the reception of the payload. This introduces the proposed two-stage tandem M/M/1/L Markov queuing model shown in Fig. 3. Please note that the term "User Equipment(s)", denoted "UEs" throughout this study, refers to any connected mobile devices on the ground.

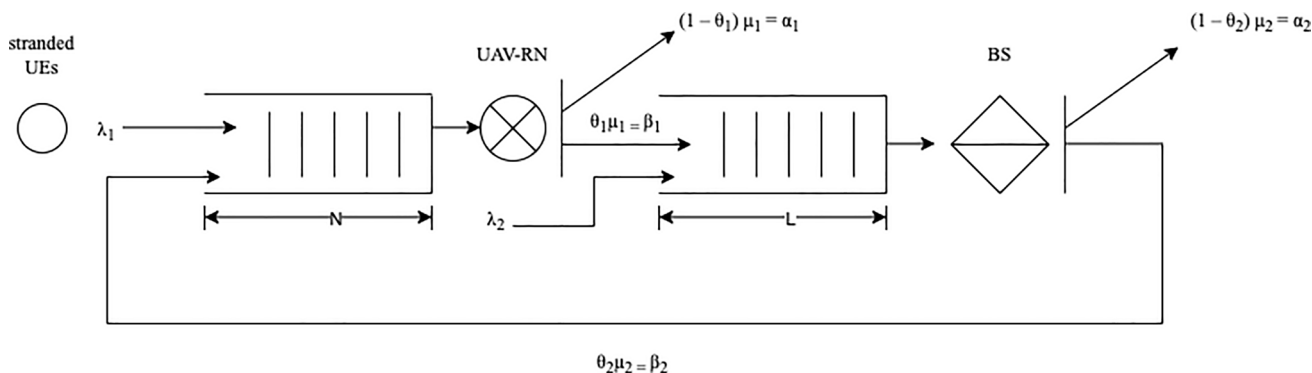


Fig. 3 Two-stage queuing model with feedback for the proposed framework

Table 2 Notations and their definitions

Notations	Definitions (trace-based)
λ_1	Mean arrival rate at the UAV relay node (from stranded UEs)
λ_2	Mean arrival rate at the (operational) Base Station (from its assigned ground devices)
μ_1	Mean service rate at the UAV relay node
μ_2	Mean service rate at the (operational) BS
θ_1	Probability of packet forwarding at the UAV-RN stage
θ_2	Probability of packet feedback at the operational BS stage
$\theta_1\mu_1$	Forwarding rate of packets from stage one (UAV-RN) to stage two (BS)
$\theta_2\mu_2$	Feedback rate of packets from stage two (BS) to stage one (UAV-RN)
$(1 - \theta_1)\mu_1$	Departure rate of packets from stage one (due to packet loss)
$(1 - \theta_2)\mu_2$	Departure rate of packets from stage two (due to service completion)
u_1	System utilisation/non-idle time portion at stage one
u_2	System utilisation/non-idle time portion at stage two
γ_1	System throughput at stage one
γ_2	System throughput at stage two
N	Queue capacity at the UAV-RN stage
L	Queue capacity at the operational BS stage
ϵ	Limit governing convergence (in the iterative solution, Sect. 4.3)

We’re using M/M/1/L queues in our model because the small SOS packets can already serve many devices quickly. In such a case, multiple servers (meaning more channels in the UAV relay node/base station) aren’t needed. The parameters used in the queuing model, whose notations are matched with their respective definitions in Table 2, can be explained as follows:

1. Arrival Rates: The primary arrivals are the packets originating from the cell represented as λ_1 for stage one and λ_2 for stage two. The inter-arrival times follow an exponential distribution [11, 30, 31]. The secondary arrivals are represented as β_1 for stage one and β_2 for stage two. These arrivals are computed as the product of $\theta_1\mu_1$ and $\theta_2\mu_2$. When packets arrive, they are served if the channel

is free. If the channel is busy, the packets go into their respective queues and wait for their turn to be served.

2. Service rates: Service times are exponentially distributed [11, 30, 31], and the service rates for stages one and two are denoted by μ_1 and μ_2 respectively. Packets from stage one may be forwarded to stage two with the probability θ_1 , or the packets may depart with the probability $(1 - \theta_1)$.
3. Forwarding probabilities: The probabilities are represented as θ_1 and θ_2 for stages one and two, respectively.
4. Queue lengths: The queue capacity of the first stage is N , and the second stage is L .

A two-dimensional Markov process can be used to represent the tandem system shown in Fig. 3. The Markov

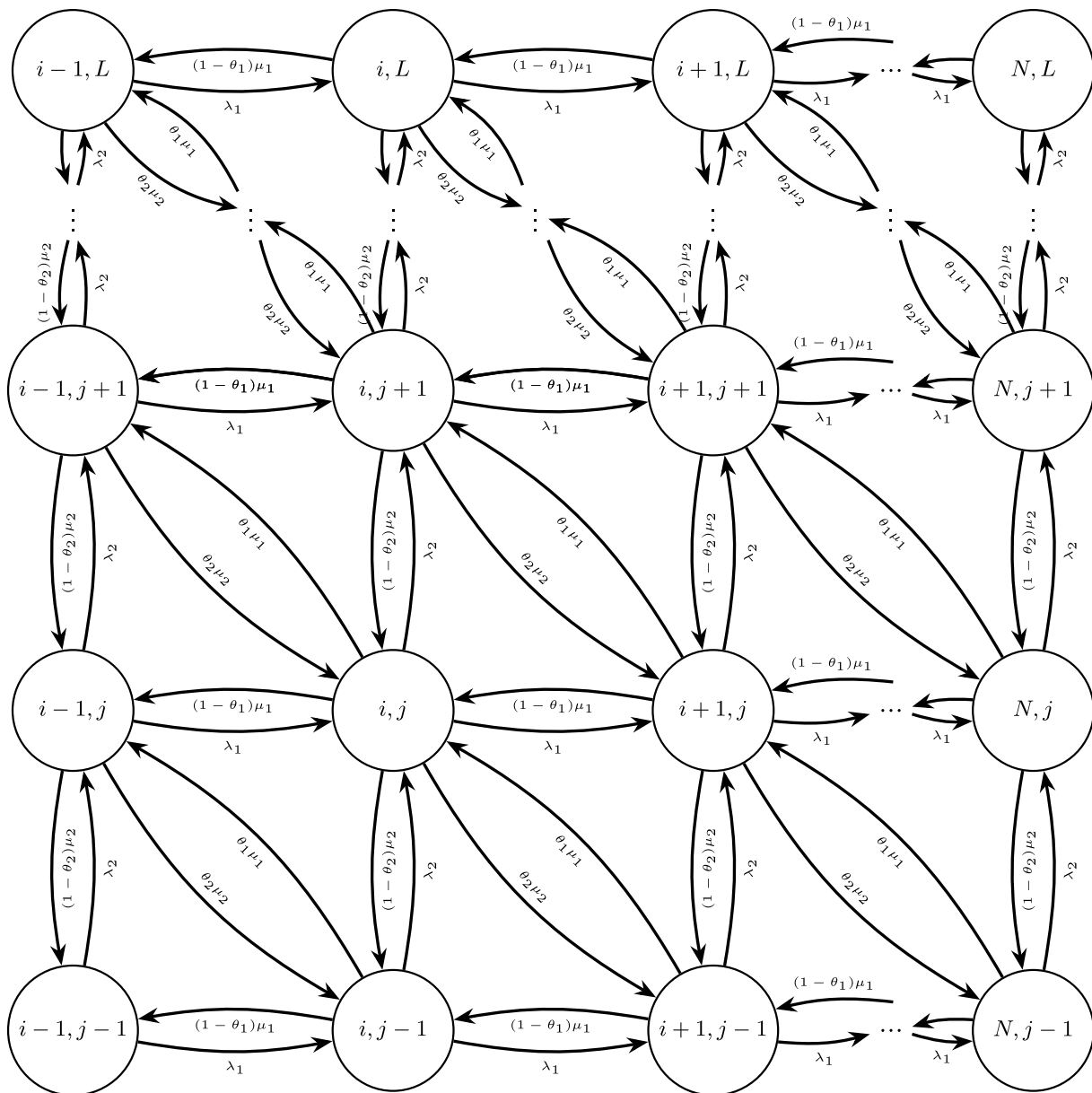


Fig. 4 State transition diagram for two-dimensional Markov processes

process can be expressed on a finite or semi-finite lattice strip as $Z = [I(t), J(t)]$ for $t \geq 0$ having a state space of size $[0, 1, 2, \dots, N] \times [0, 1, 2, \dots, L]$ [11, 31, 32]. Z is an irreducible Markov process to represent the number of packets in the UAV-RN and BS queuing stages, respectively. The state diagram is illustrated in Fig. 4. In the state transition diagram, the system state is denoted/described by the variables i (the instantaneous number of packets in the UAV-RN stage of the tandem queues) and j (the instantaneous number of packets in the BS stage of the tandem queue). The horizontal transitions represent a change in the first

stage, while vertical transitions represent a change in the second stage.

For a rough idea of the logic of the transition diagram, consider the state labelled (i, j) in Fig. 4. The upward transition would increment j . This translates to an originating packet within the cell of the operational base station, i.e., a primary arrival in the second stage denoted by λ_2 . This transition logic spawns the two-dimensional lattice that allows us to trace the behaviour of our queuing model given different stimuli denoted in Table 2.

Considering the two-dimensional Markov process in Fig. 4, it is possible to derive the balance equations that

can be used to compute the state probabilities, $P(i, j)$, for each region of the state transition diagram as follows:

Region 1: where $i = 0, j = 0$

$$P_{0,0} = \frac{P_{1,0} * \alpha_1 + P_{0,1} * \alpha_2}{\lambda_2 + \lambda_1} \tag{1}$$

Region 2: where $i = 0, j = L$ (maximum capacity for the relay stage);

$$P_{0,L} = \frac{P_{0,L-1} * \lambda_2 + P_{1,L} * \alpha_1 + P_{1,L-1} * \beta_1}{\lambda_1 + \beta_2 + \alpha_2} \tag{2}$$

Region 3: where $i = N$ (maximum capacity for the up-link stage), $j = L$ (maximum capacity for the relay stage);

$$P_{N,L} = \frac{P_{N-1,L} * \lambda_1 + P_{N,L-1} * \lambda_2}{\alpha_2 + \alpha_1} \tag{3}$$

Region 4: where $i = N$ (maximum capacity for the up-link stage), $j = 0$;

$$P_{N,0} = \frac{P_{N-1,0} * \lambda_1 + P_{N-1,1} * \beta_2 + P_{N,1} * \alpha_2}{\alpha_1 + \beta_1 + \lambda_2} \tag{4}$$

Region 5: where $i = 0, 0 < j < L$ (maximum capacity for the relay stage);

$$P_{0,j} = \frac{P_{0,j+1} * \alpha_2 + P_{1,j} * \alpha_1 + P_{0,j-1} * \lambda_2 + P_{1,j-1} * \beta_1}{\beta_2 + \lambda_2 + \lambda_1 + \alpha_2} \tag{5}$$

Region 6: where $0 < i < N$ (maximum capacity for the up-link stage), $j = L$ (maximum capacity for the relay stage);

$$P_{i,L} = \frac{P_{i,L-1} * \lambda_2 + P_{i-1,L} * \lambda_1 + P_{i+1,L} * \alpha_1 + P_{i+1,L-1} * \beta_1}{\alpha_1 + \lambda_1 + \beta_2 + \alpha_2} \tag{6}$$

Region 7: where $i = N$ (maximum capacity for the up-link stage), $0 < j < L$ (maximum capacity for the relay stage);

$$P_{N,j} = \frac{P_{N-1,j} * \lambda_1 + P_{N,j-1} * \lambda_2 + P_{N,j+1} * \alpha_2 + P_{N-1,j+1} * \beta_2}{\lambda_2 + \alpha_1 + \alpha_2 + \beta_1} \tag{7}$$

Region 8: where $0 < i < N$ (maximum capacity for the up-link stage), $j = 0$;

$$P_{i,j} = \frac{P_{i-1,0} * \lambda_1 + P_{i,1} * \alpha_2 + P_{i+1,0} * \alpha_1 + P_{i-1,1} * \beta_2}{\alpha_1 + \lambda_2 + \lambda_1 + \beta_1} \tag{8}$$

Region 9: where $0 < i < N$ (maximum capacity for the up-link stage), $0 < j < L$ (maximum capacity for the relay stage);

$$P_{i,j} = \frac{P_{i,j-1} * \lambda_2 + P_{i-1,j} * \lambda_1 + P_{i-1,j+1} * \beta_2 + P_{i,j+1} * \alpha_2 + P_{i+1,j} * \alpha_1 + P_{i+1,j-1} * \beta_1}{\alpha_1 + \beta_1 + \lambda_2 + \lambda_1 + \alpha_2 + \beta_2} \tag{9}$$

All possible states in the lattice fall under one of the above nine regions whose state probabilities are expressed in Eqs. 1 to 9.

3.2.1 System of simultaneous equations solution

It is possible to solve the system of balance equations with $(N + 1) \times (L + 1)$ state probabilities using various methods. **A** can be defined as a matrix of instantaneous transition rates that holds the coefficients of the system of simultaneous equations of all state probabilities. We can solve this system for the state probabilities by considering the equation $\mathbf{AX} = \mathbf{B}$, where the matrix **X** holds the state probability variables (P_{ij} 's) and matrix **B** holds the result of the equations (in our case, this matrix will hold zeros for all the equations except normalisation equation which states that the sum of all P_{ij} 's is 1).

In this study, we employed the effective *numpy* libraries in Python to implement this particular method and solve for state probabilities from the system of simultaneous equations. This solution requires solving the system of $(N + 1) \times (L + 1)$ simultaneous equations to obtain the $(N + 1) \times (L + 1)$ state probabilities. Although the performance measures computed using this solution are within the desired error margin of 5% consistent with the confidence interval of the simulation program, the method proves to be severely computationally heavy for queue sizes above $(150 + 1) \times (150 + 1)$. To this effect, we shall introduce a more computationally sound *iterative solution*.

4 The iterative solution

Having presented the queuing model and an accompanying solution, it would be prudent to expand the solution to fit a more realistic implementation. The general procedure for the iterative solution [12] can be given as follows:

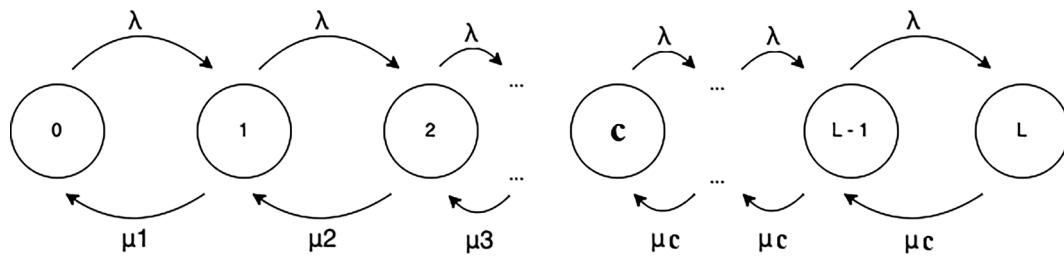


Fig. 5 State transition diagram for M/M/c/L queue

1. Initial conditions for $P(i, j)$ for $i = 0, 1, 2, 3, \dots, N$ and $j = 0, 1, 2, 3, \dots, L$ are calculated using various approaches and Markov process logic.
2. The balance equations given in Eq. 1 to Eq. 9 are used to calculate the correct steady state probabilities.
3. Various performance measures, such as Mean queue length (MQL), can be calculated for the queuing system considered.
4. Second and third steps are repeated until the selected performance measure (MQL for our case) converges sufficiently as per the chosen limit of convergence, ϵ .

4.1 Initial conditions

Consider an example with the state transition diagram shown in Fig. 5 for a simple Markov M/M/c/L queue with Markov exponentially distributed inter-arrival times and service times.

Taking constant arrival (λ) and service (μ_i 's, for $1 \leq i \leq c$, and $\mu_i = i\mu$) rates, we can derive the state probabilities as follows;

$$P_0 = \frac{1}{\left(\sum_{i=0}^{c-1} \frac{1}{i!} * \rho^i\right) + \left(\sum_{i=c}^L \frac{1}{c!} * \frac{1}{c^{(i-c)}} * \rho^i\right)} \tag{10}$$

We can then calculate the state probabilities of the individual M/M/1/L (noting that $c = 1$ in our case) queues that constitute our tandem queuing model in Fig. 3 as follows:

for $i < c$,

$$P_i = \frac{1}{i!} * \rho^i * P_0 \tag{11}$$

and for $i \geq c$

$$P_i = \frac{1}{c!} * \frac{1}{c^{(i-c)}} * \rho^i * P_0 \tag{12}$$

Using the state probabilities, P_i 's for $i = 0, 1, 2, 3, \dots, N$ and P_j 's for $j = 0, 1, 2, 3, \dots, L$, we can obtain the initial values of the state probabilities for our two-dimensional Markov process, $P_{i,j}$'s, by following the well known Markov Reward Modelling approach [33] and cross multiplying the state probabilities of the up-link and relay stages such that $P_{i,j} = P_i * P_j$ for $i = 0, 1, 2, 3, \dots, N$ and $j = 0, 1, 2, 3, \dots, L$.

4.1.1 Accounting for relaying and feedback

Please note that the approximate state probabilities computed to set the initial conditions do not account for the forwarding and feedback probabilities (θ_1 and θ_2).

It is possible to adapt the use of an effective arrival rate (denoted as λ_e) from [11] similarly maintained below $c\mu_1$ (i.e., μ_1 since $c = 1$) for the system to be at stable state. Another imperative point to note is that we will apply the use of λ_e in calculating the initial P_i and P_j state probabilities using Eqs. (11) and (12) to propagate the effect of θ_1 and θ_2 throughout the queue contrary to its application to the first stage only in [11]. The derivation of λ_e for the introduced tandem system comprising two M/M/c/L queues (where

Table 3 Derivation of effective arrival rate, λ_e

Iteration	Feedback	Effective arrival rate, λ_e
0		λ
1	$\lambda\theta$	$\lambda + \lambda\theta = \lambda(1 + \theta)$
2	$\lambda(1 + \theta)\theta$	$\lambda + \lambda\theta + \lambda\theta^2 = \lambda(1 + \theta + \theta^2)$
3	$\lambda(1 + \theta + \theta^2)\theta$	$\lambda + \lambda\theta + \lambda\theta^2 + \lambda\theta^3 = \lambda(1 + \theta + \theta^2 + \theta^3)$
.	.	.
.	.	.
.	.	.
i	$\lambda(1 + \theta + \theta^2 + \dots + \theta^i)$	$\lambda \sum_{n=0}^i \theta^n$

$c = 1$) follows the iterative logic in Table 3 and the subsequent Eqs. (13) to (19) below:

From the above, we can arrive at the conclusion that;

$$\lambda_e = \lambda \sum_{n=0}^{\infty} \theta^n; \tag{13}$$

which we can then express as,

$$\lambda_e = \lambda * \frac{1}{1 - \theta} = \frac{\lambda}{1 - \theta} \tag{14}$$

Expanding this notation for the two-stage queuing for which we are modelling, we can express the effect of θ_1 and θ_2 as;

$$\lambda_e = \lambda_1 + \lambda_1 \theta_1 \theta_2 + \lambda_2 \theta_2 \dots \tag{15}$$

$$\lambda_e = \lambda_1 + \lambda_1 \theta_1 \theta_2 + \lambda_1 (\theta_1 \theta_2)^2 + \lambda_2 \theta_1 \theta_2^2 + \lambda_2 \theta_2 \dots \tag{16}$$

$$\lambda_e = \lambda_1 + \lambda_1 \theta_1 \theta_2 + \lambda_1 (\theta_1 \theta_2)^2 + \lambda_1 (\theta_1 \theta_2)^3 + \lambda_2 \theta_1^2 \theta_2^3 + \lambda_2 \theta_1 \theta_2^2 + \lambda_2 \theta_2 \dots \tag{17}$$

$$\begin{aligned} \lambda_e &= \lambda_1 \sum_{n=0}^i (\theta_1 \theta_2)^n + \lambda_2 \theta_2 \sum_{n=i}^0 (\theta_1 \theta_2)^n; \lambda_e \\ &= \lambda_1 \sum_{n=0}^l (\theta_1 \theta_2)^n + \lambda_2 \theta_2 \sum_{i=n}^0 (\theta_1 \theta_2)^n \end{aligned} \tag{18}$$

since the above series notation can be expressed as

$$\sum_{n=0}^L (\theta_1 \theta_2)^n = \frac{1}{1 - \theta_1 \theta_2},$$

λ_e can ultimately be contracted into the formula;

$$\lambda_e = \frac{\lambda_1 + \lambda_2 \theta_2}{1 - \theta_1 \theta_2} \tag{19}$$

This hitherto derived effective arrival rate, λ_e , is the value used to calculate the initial state probabilities, P_i 's and P_j 's (of the individual M/M/1/L queues comprising our two-stage model) required for step (i) mentioned in the description of the iterative solution at the start of Sect. 4. We now have the parameters required to set up the initial conditions that will kick off our iterative model.

4.2 Performance measures

The performance measures tracked to verify the validity of the proposed queuing model in this study are the mean queue length, throughput and response time. Equations (20) to (25) are used to obtain the analytical results of the above queuing performance from the state probabilities,

P_{ij} 's, at which the model will have converged at the end of the iterative run.

Mean queue length at the UAVRN stage,

$$MQL_{UAVRN} = \sum_{j=0}^L j \sum_{i=0}^N P_{i,j} \tag{20}$$

Mean queue length at the BS stage,

$$MQL_{BS} = \sum_{i=0}^N i \sum_{j=0}^L P_{i,j} \tag{21}$$

Throughput at the UAVRN stage,

$$\gamma_1 = \mu_1 (1 - \sum_{j=0}^L P_{0,j}) \tag{22}$$

Throughput at the BS stage,

$$\gamma_2 = \mu_2 (1 - \sum_{i=0}^N P_{i,0}) \tag{23}$$

Response time at the UAVRN stage,

$$RT_{UAVRN} = \frac{MQL_{UAVRN}}{\gamma_1} \tag{24}$$

Response time at the BS stage,

$$RT_{BS} = \frac{MQL_{BS}}{\gamma_2} \tag{25}$$

4.3 Convergence

Following step (iv) of the iterative method, the next phase of the iterative solution simply involves running the loop that is used to assign the state probabilities, P_{ij} 's, using the Eqs. (1) to (9) with the term P_{ij} as the subject of the formulae. As explained in 3.2, the aforementioned balance equations cater for all the possible regions in the 2d transition lattice in Fig. 4 that results from the implementation of the proposed two-stage queue.

The number of iterations required is governed by the formulae used to check for convergence after each iteration; ($|MQL_{old} - MQL_{new}| < \epsilon$). It would be prudent to note that the stability of the system, i.e., utilisation $u \leq 1$ and the sum of all state probabilities, P_{ij} 's ≈ 1.0 , is maintained throughout the run of the iterative analytical solution.

4.4 The simulation program

The **in-house** simulation program used to validate the results of the analytical model and the iterative solution approach

in terms of accuracy as well as efficacy is similar to the ones used in studies such as [1, 11, 34, 35]. The results obtained from the analytical model and the iterative solution approach are presented comparatively with the results from simulation software written in C++ language and validated to simulate the actual system. The simulation program developed is validated using established queuing theory models such as M/M/1, and M/M/c as well as results from the literature [34, 35].

We use a discrete event simulation program that relies on an event-based scheduling approach. This approach depends on events and their impact on the system state. We use relative precision, a commonly employed stopping criterion in simulations. In this approach, we halt the simulation at the first checkpoint once the condition $\delta \leq \delta_{max}$ is satisfied. Here, δ_{max} represents the highest allowable value for relative precision of confidence intervals at a $100(1 - \alpha)\%$ significance level, where $0 < \delta_{max} < 1$. Our simulation results fall within the 5% confidence interval with a 95% confidence level. As a result, we set both α and δ to 0.05 as the default values in the simulation.

5 Results and discussions

This section presents the results obtained from the iterative analytical solution compared and contrasted with the simulation results. Discussion of the trends observed in the results obtained and accompanying explanations are provided.

5.1 System parameters

In line with proposed models used for heterogeneous networks, the radius of the cell is taken to be 1000 m [36], and the line-of-sight range/radius of coverage of the UAV-RN is taken to be that of a standard disaster management/search and rescue drone at 1000 m [37]. The maximum velocity, V_{max} , of the Intel Aero Ready-to-Fly drone, is taken to be 15 m/s from [38]. Nonetheless, our assumption rests on the premise that the drone's consistent and often overlapping coverage as it moves along the cell border, along with the minimalistic nature of the SOS packets, effectively mitigates the direct influence of the UAV-RN's speed on the arrival and service rates, and thus, the performance metrics of the queuing model.

Indeed, taking an example of a scenario where the probability of relaying from stage one to stage two, θ_1 , is 0.6, the probability of a miss (due to line-of-sight issues, poor physical conditions caused by the ongoing disaster or its aftermath, signal attenuation due to the UAV-RN having to fly at a higher altitude than the optimum, etc) would be $1 - \theta_1$ i.e., 0.4. Each of the ground devices is broadcasting

its SOS packet in a heartbeat rhythm every second (in this example) as indicated in the assumptions discussed in 3.1, with the UAV traversing the sub-cell (ideally the 1km length of the side of the macro-cell) at a velocity, V_{max} , of 15m/s consequently providing continuous coverage to the stranded devices. The UAV would provide coverage for up to 66.667s thus still being able to pick up the SOS packets. This follows the fact that the probability that all twenty tries (one for each second) are misses exponentially decreases towards a negligible value with each broadcast attempt (in this case, the probability of all twenty broadcasts being misses would be 0.4^{20}). We can, therefore, safely assert that the likelihood of an SOS packet not being received during a traversal is down to factors not to do with the operational parameters of the UAV-RN, thus outside of our control as pertains to this study.

The physical layer parameters of the drone are incorporated in the system parameters, especially the UAV-RN service rate, μ_1 , specified throughout this section. As the available literature on queue modeling in this specific context is scarce, we have chosen the majority of the queuing parameters in this study based on comprehensive research from which we developed the proposed solution, as referenced in [1, 11, 12]. This, naturally, assumes that the system's stability aligns with the mathematical assumptions of Markov models.

Based on the assumption that the proposed framework is designed to be reliable and not reliant on the existing channel infrastructure, the UAV-RN and the base station have single channels, with the latter designated as an emergency channel that remains otherwise unused. We can allocate an unused channel to the base station because even with high queue capacities, the size of the SOS packets, as discussed in Sect. 3.1 is considerably smaller than standard data packets. Consequently, it is expected that the bandwidth required for this channel would be significantly lower, albeit consistently used. Therefore, the overhead cost associated with maintaining this channel when not in use is anticipated to have a negligible impact on the performance of the base station link during normal operations.

The **standard** queue capacity for the emergency channel at the operational base station and the UAV-RN is set at 1500 packets [39]. The usual arrival rate at the UAV-RN stage, denoted as λ_1 , is 500 packets per second, while at the emergency channel of the operational base station, denoted as λ_2 , it is also 500 packets per second. The conventional service rate at the UAV-RN stage, labelled as μ_1 , is 2000 packets per second, while at the emergency channel of the operational base station, labelled as μ_2 , it is 1000 packets per second. In following subsections, we have examine various relaying probabilities (θ 's), arrival rates (λ 's), and service rates (μ 's) within the limits of system stability when evaluating the iterative model.

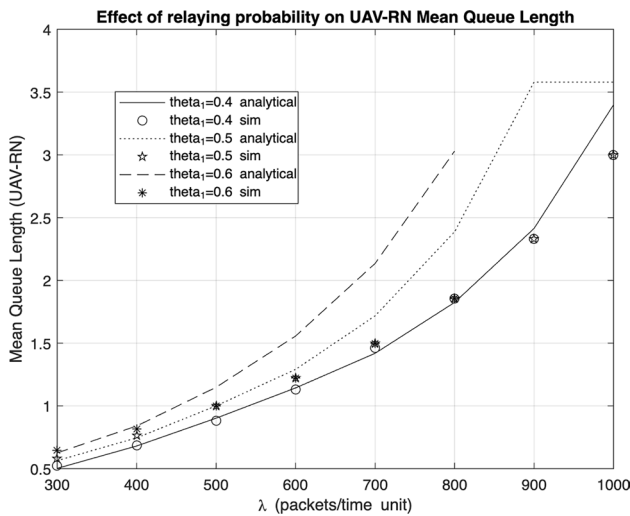


Fig. 6 Effect of θ_1 on UAV-RN Mean Queue Length

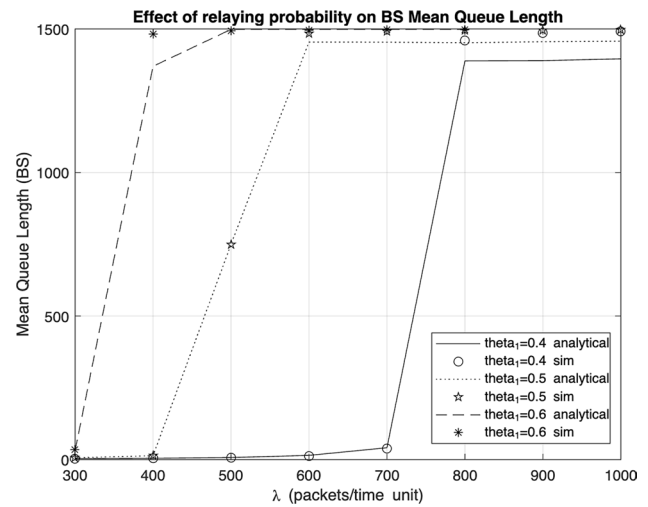


Fig. 8 Effect of θ_1 on BS Mean Queue Length

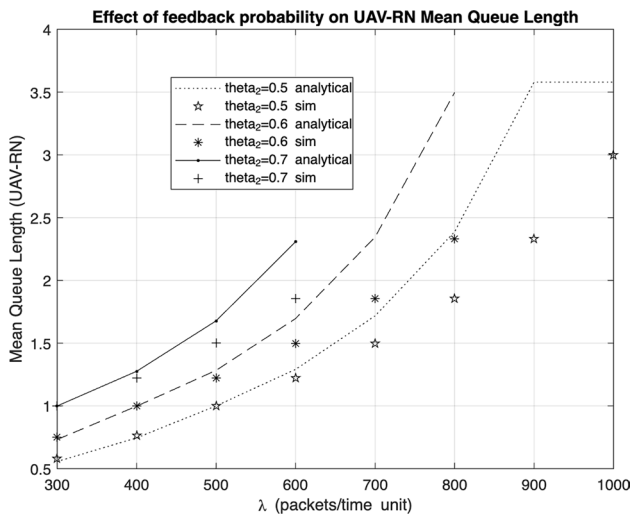


Fig. 7 Effect of θ_2 on UAV-RN Mean Queue Length

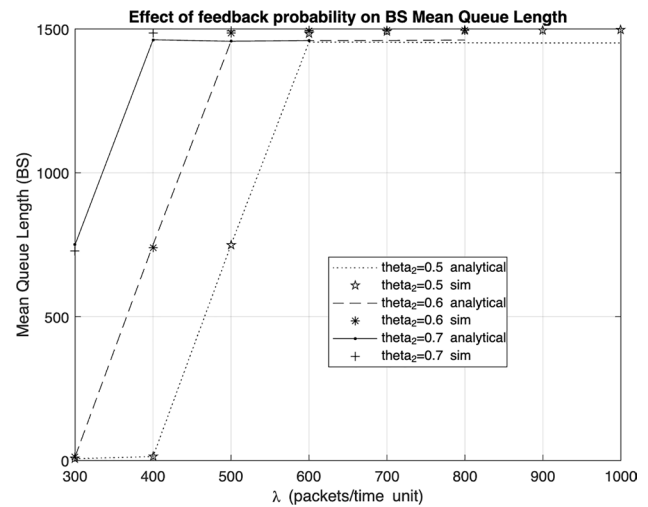


Fig. 9 Effect of θ_2 on BS Mean Queue Length

5.2 Numerical results

The graphs are labelled and separated by order of performance measure (mean queue length, throughput then response time) for ease of reading as well as comparison. Accompanying discussions are provided to aid in comprehension.

The set of graphs below (Figs. 6, 7, 8, 9, 10, 11, 12, 13, 14, 15, 16 and 17) show the effect of relaying probability, θ_1 , and feedback probability, θ_2 , on the selected performance measures - mean queue length, throughput and response time. To investigate the effect of θ_1 , we have maintained the standard system parameters specified in the previous Sect. (5.1) while increasing the value of λ_1 until the system is no longer stable.

Regarding the mean queue length at the UAV-RN stage, denoted as MQL_{UAVRN} , a notable trend is the consistent increase in mean queue length as λ_1 increases. This is to be expected due to the high service rate at the UAVRN stage, μ_1 , capped at a constant value of 2000 packets per second. Moreover, from the graphs contrasting MQL_{UAVRN} results for the analytical and simulation models (Fig. 6 for θ_1 ; Fig. 7 for θ_2), we can identify the jump point of each of the performance measures for each θ_1 value. The “jump point” (to which we have also referred interchangeably as **critical λ_1**) refers to the λ_1 value at which the mean queue length of the UAV-RN and/or the BS stage jumps to a value very close to the respective queue capacity limit (N or L respectively) thus causing the system to approach instability. In

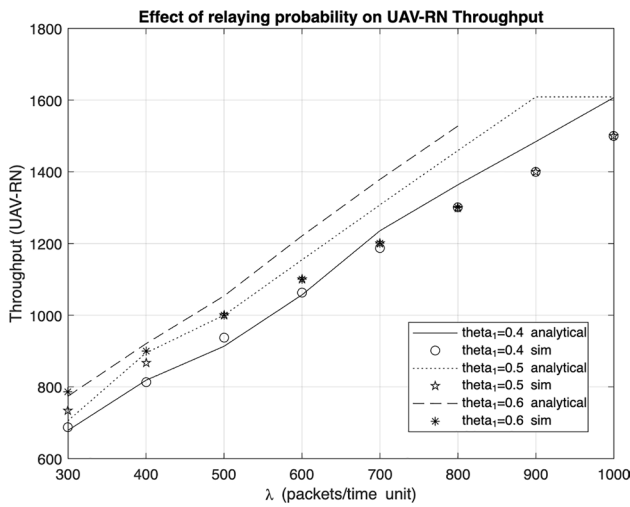


Fig. 10 Effect of θ_1 on UAV-RN Throughput

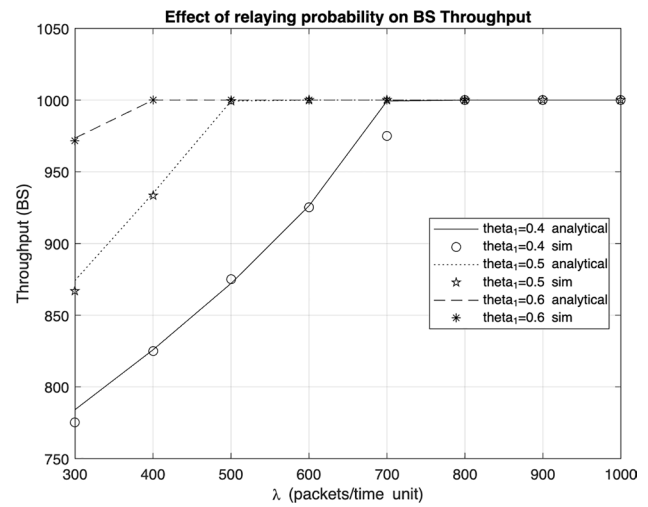


Fig. 12 Effect of θ_1 on BS Throughput

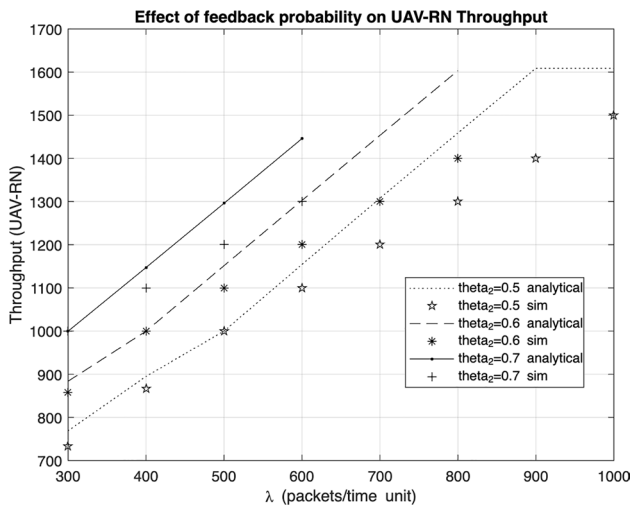


Fig. 11 Effect of θ_2 on UAV-RN Throughput

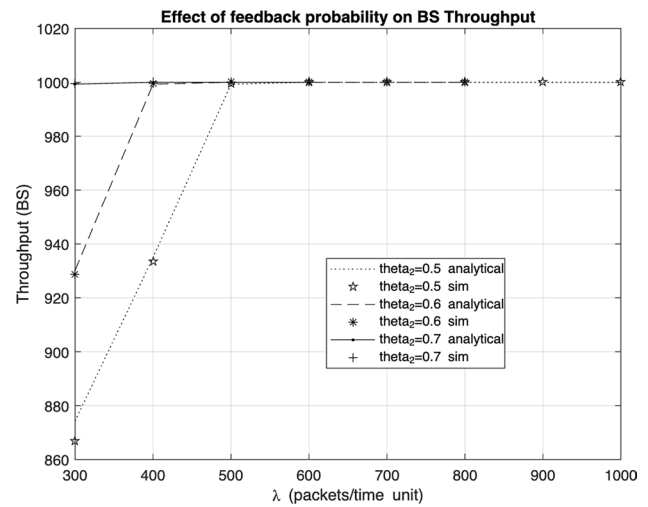


Fig. 13 Effect of θ_2 on BS Throughput

the graphs depicting the impact of θ_1 on the mean queue length of the UAV-RN stage, this point is marked by a clear divergence between the simulation and analytical model plots. At this λ_1 value, the mean queue length substantially approaches the maximum queue capacity, either in the first stage or both, signalling the system’s approach to instability. For the range of stable λ_1 values, the maximum discrepancy between the analytical and simulation values exhibited was 4.0313%. Upon further observation, it is also notable that the λ_1 value at which the jump occurs decreases with increasing θ_1 value; at 600 packets per second when $\theta_1 = 0.4$, 500 packets per second when $\theta_1 = 0.5$, 400 packets per second when $\theta_1 = 0.6$.

The chosen θ_1 values and λ_1 range never push stage one’s MQL to the queue capacity limit, N , thanks to its constant high service rate of 2000 packets per second. In contrast, stage two consistently reaches the queue capacity before stage one due to its lower service rate, which is limited to 1000 packets per second. The critical λ_1 value explored in this section is primarily determined by the sudden rise in stage two’s MQL values.

Regarding feedback probability θ_2 , in Fig. 7, the critical λ_1 value, where the simulation and analytical plots start to diverge, demonstrates a maximum discrepancy of 3.7391% for stable λ_1 values. This divergence occurs when the MQL of the second stage suddenly approaches the queue capacity limit L , leading to system instability. Maintaining a θ_1 value of 0.5 while studying the impact of

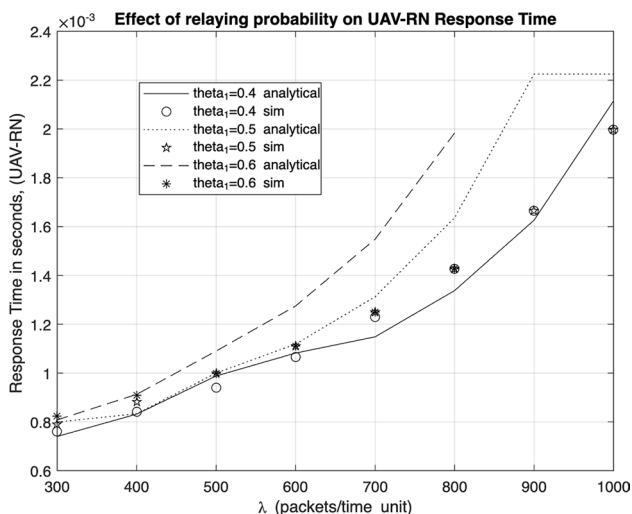


Fig. 14 Effect of θ_1 on UAV-RN Response Time (in seconds)

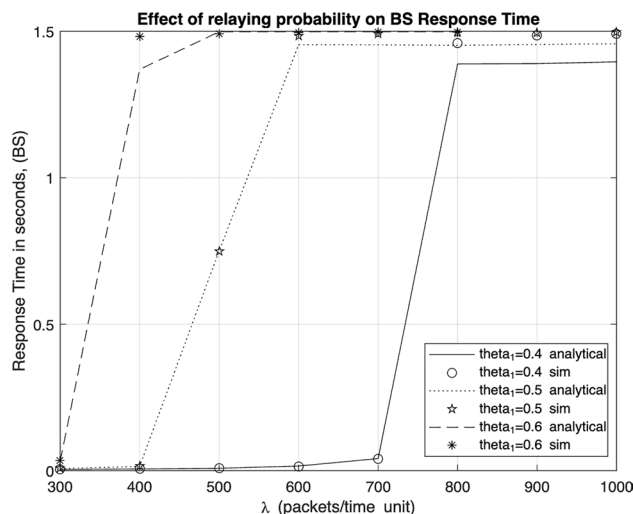


Fig. 16 Effect of θ_1 on BS Response Time (in seconds)

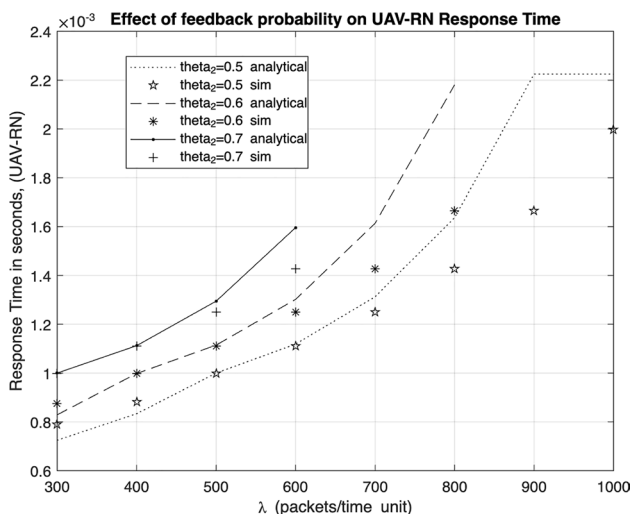


Fig. 15 Effect of θ_2 on UAV-RN Response Time (in seconds)

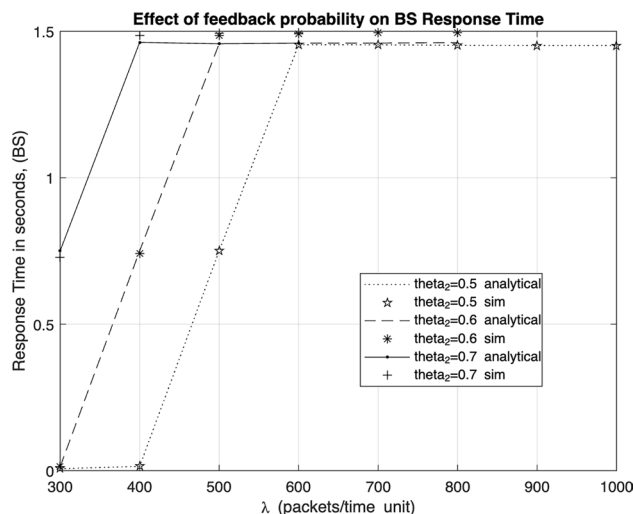


Fig. 17 Effect of θ_2 on BS Response Time (in seconds)

θ_2 yields identical critical λ_1 values as those obtained in the study of θ_1 . The choice of $\theta_1 = 0.5$ is based on the previously discussed results, where an MQL value of 750 at the second stage with $\lambda_1 = 500$ packets per second strikes a balance between system utilization and stability. This confirms the suitability of the standard parameters mentioned in the “System Parameters” section (5.1).

Considering the mean queue length at the BS stage, denoted as MQL_{BS} , the trends are highly predictable. Similar to the behaviour observed in previous work on the impact of vertical upward handover on femtocell mean queue length [11], the graphs (see Fig. 8 for θ_1 and Fig. 9 for θ_2) clearly show that as λ_1 increases, the MQL value rises until it reaches a critical point, after which it plateaus as it approaches the queue capacity limit L , resulting in system

instability. In this analysis, the maximum deviation between analytical and simulation results was 4.0212%.

Similar to the impact of θ_1 , the noticeable effect of feedback probability θ_2 is that the critical λ_1 value is reached more rapidly with increasing θ_2 . This is particularly evident when $\theta_2 = 0.7$, where the system quickly becomes unstable. This reinforces the choice of the standard value of 0.5 for our relaying and feedback probabilities. In this analysis, the maximum deviation between analytical and simulation results was 2.6687

UAV-RN stage throughput, denoted as γ_1 , is shown in Fig. 10 for θ_1 and Fig. 11 for θ_2 , both simulation and analytical model results indicate that the throughput at the first stage increases with rising λ_1 , but then diverges after reaching the critical λ_1 . The critical λ_1 can be identified where the

simulation and analytical model values diverge. Up to this point, while the system is stable, the maximum discrepancy between the simulation and analytical approach is 3.78261.

The same observation applies to the effect of θ_2 , with the added observation that the steadily increasing high throughput values approach the maximum queue capacity, N for the UAV-RN stage and L for the BS stage due to the relatively high service rates and the increasing incoming packets governed by λ_1 .

The throughput at the BS stage is denoted as γ_2 . Figure 12 for θ_1 and Fig. 13 for θ_2 shows that the behaviour of the second stage throughput remains consistent across different θ_1 values. The throughput increases steadily with growing λ_1 but levels off after surpassing the critical λ_1 values, coinciding with the point where the MQL of stage two approaches the queue limit L as the system becomes unstable. This rise in throughput is attributed to the increasing packet flow through UAV-RN due to a continuous influx of packets. Similar to θ_1 , the impact of θ_2 on the second stage’s throughput results in an earlier plateau with higher θ values. This plateau aligns with the jump point observed in the graphs depicting the effect of θ_1 and θ_2 on mean queue length.

Concerning the response time at the UAV-RN stage, denoted as RT_{UAVRN} , it consistently increases with higher λ_1 values, reflecting the greater influx of packets per unit of time. However, the response times at the first stage remain low due to the high service rate. The behaviour of response time closely mirrors the mean queue length (Fig. 14 for θ_1 and Fig. 15 for θ_2). This similarity persists up to the critical λ_1 , after which the MQL of the second stage rapidly rises to values approaching the queue capacity limit as the system becomes unstable.

The impact of both θ_1 and θ_2 on the response time of stage one is comparable, as evidenced by Figs. 14 and 15. In both cases, simulation and analytical results diverge after reaching the critical λ_1 for each θ value. This divergence occurs as the system approaches instability, primarily due to the

MQL of the second stage sharply rising to values near the maximum queue capacity.

The response time at the BS stage is denoted as RT_{BS} and is considered in Figs. 16 and 17. It follows a steady increase with the growing influx of packets at stage one, reaching the critical λ_1 sooner due to the higher packet rate. This can be attributed to the effect of higher θ_1 values. With higher θ_1 more packets are forwarded to the second stage, and since θ_2 is held constant at 0.5, more packets are fed back to the first stage, leading to system instability by accumulating packets and increasing response time. The same principle applies when increasing θ_2 . Raising θ_2 while maintaining θ_1 at 0.5 results in more packets being fed back to stage one, causing packet accumulation and a corresponding increase in response time.

Increasing the relaying probability, θ_1 narrows the acceptable range of primary arrival rates, λ_1 . This is anticipated because a higher θ_1 leads to more packets being relayed to the second stage, causing the second stage to reach instability at a lower λ_1 value. For example, with $\theta_1 = 0.4$, the range of arrival rates extends up to 1000 packets per second, beyond which the system becomes unstable. This limit remains at 1000 packets per second with $\theta_1 = 0.5$, but it decreases to 800 packets per second when $\theta_1 = 0.6$.

In the subset of graphs depicting the behaviour of the second (BS) stage, the system quickly becomes unstable when both θ_1 and θ_2 are set to 0.7. This aligns with our earlier observation that the critical λ_1 steadily decreases with higher values of both θ_1 and θ_2 , making the use of 0.7 as the relaying probability impractical.

Regarding the effect of θ_2 an increase in the feedback probability leads to a greater number of packets forwarded to the BS stage, even when θ_1 is held constant. This, in turn, fills the second stage more rapidly, especially considering the lower service rate, μ_2 , capped at 1000 packets per second.

Table 4 Effect of [stable range of] UAV-RN service rates, μ_1 , on Mean Queue Length

μ_1	MQL_{UAVRN}			MQL_{BS}		
	Iterative	Simulation	% discrepancy	Iterative	Simulation	% discrepancy
1000	750	722.3676	3.825254621	750	717.3996	4.544245634
1100	10	9.9396	0.017913208	750	745.1917	0.645243365
1200	5	4.9855	0.016892853	750	723.9994	3.59124607
1300	3.3333	3.3254	0.018793531	750	745.9461	0.543457496
1400	2.5	2.4947	0.017092921	750	743.785	0.83559093
1500	2	1.9962	0.023135351	750	722.9704	3.73868695
1600	1.66667	1.6639	0.01640269	750	747.1679	0.379044656
1700	1.42857	1.4264	0.020054021	750	735.3434	1.99316401
1800	1.25	1.2484	0.016932867	750	739.9751	1.354761802
1900	1.11111	1.1095	0.020734298	750	733.5722	2.239425104
2000	1	0.999	0.018673486	750	730.4561	2.675574891

Table 5 Effect of [stable range of] BS service rates, μ_2 , on Mean Queue Length

μ_2	MQL_{UAVRN}			MQL_{BS}		
	Iterative	Simulation	% discrepancy	Iterative	Simulation	% discrepancy
1200	750	746.3011	0.495631053	5	4.997	0.645243365
1400	750	731.7714	2.491023836	2.5	2.4972	3.59124607
1600	750	738.2025	1.598138722	1.66667	1.6658	0.543457496
1800	750	734.7447	2.076272207	1.25	1.2489	0.83559093
2000	750	747.6664	0.023135351	1	0.9995	3.73868695
2200	750	748.6592	0.01640269	0.83333	0.8329	0.379044656
2400	750	743.0074	0.020054021	0.714286	0.7139	1.99316401

Table 6 Contrasting CPU run times (in seconds) for testing the range of stable μ_1

μ_1	$RunTime_{Iterative}$	$RunTime_{Simulation}$
700	0.386391	239.22
800	0.395816	250.77
900	0.388788	259.79
1000	0.385237	317.49
1100	0.386434	253.03
1200	0.366956	252.93
1300	0.385981	252.74
1400	0.394706	252.07
1500	0.387878	250.98
1600	0.353647	249.73
1700	0.459266	250.64
1800	0.476825	249.37
1900	0.438693	247.89
2000	0.346084	247.93

Overall, the results for both the UAV-RN and BS stages exhibit similar trends when considering the effects of relaying probability, θ_1 , and feedback probability, θ_2 . The reason for employing a lower standard service rate at the BS stage (1000 packets/second) compared to the standard service rate at the UAV-RN stage (2000 packets/second) is to illustrate the system’s behavior as it approaches the critical λ_1 and enters instability. This results in a gradual increase as the incoming packet rate approaches the critical rate, a sudden jump at the critical λ_1 and a subsequent plateau as the MQL of the BS stage nears the queue limit, L . This trend also applies to the response time. It is worth noting that the difference in service rates ensures that the UAV-RN stage is never overwhelmed, as the BS stage primarily determines the system’s stability. Consequently, the UAV-RN queue limit, N , is not reached, at least under the given parameters.

To track the effect of the service rates on the MQL, Tables 4 and 5 are used, with $\lambda_1 = 500$, $\mu_1 = 1000$, $\lambda_2 = 500$, $\theta_1 = 0.5$, $\theta_2 = 0.5$, $N = 1500$, $L = 1500$. Table 4 shows that as μ_1 increases, MQL_{UAVRN} decreases because more packets are served per unit of time. Meanwhile, MQL_{BS} oscillates around

750 (as discussed in the context of the effects of θ_1 and θ_2 on MQL), indicating an optimisation point for the system’s resources with the standard parameters. The standard service rate for the UAV-RN is set at 2000 packets per second, equivalent to 0.6 Mbps with 35 – byte SOS packets. This is a reasonable demand for a network expected to operate on 4G, 5G, or future-generation wireless infrastructure. As long as the parameters adhere to the study’s findings, the network is unlikely to become overwhelmed. To this effect, expecting the framework to facilitate this maximum service rate at the UAV-RN would not be a significant impediment as it improves efficiency by a great deal.

Table 5 shows that for the range μ_2 values for which both stages of the system are stable, the MQL of the BS decreases gradually with an increase in service rate as expected due to more packets leaving this stage per time unit. The MQL at stage one is, however, somewhat oscillates at 750 packets. Similar to the effect of μ_1 on the MQL explored in Table 4, this could be attributed to chosen θ_1 and θ_2 values, both capped at 0.5.

At this point, we can compare the temporal computational performance of the analytical solution against the custom simulation used for validating the model. Table 6 compares the CPU run-times of the iterative analytical model with that of the simulation program. The computer architectural specifications of the machine used for the analytical solution were as follows: Processor - 2.7 GHz Quad-Core Intel Core i7, Memory (RAM) - 16 GB 2133 MHz LPDDR3 (Low-Power Double Data Rate 3). The results clearly show that the proposed iterative solution consistently outperforms the simulation program. The MQL values in the analytical solution converged within a few iterations, given ϵ as 0.001. Further affirming the validity of this set of values as our standard operating parameters.

To track the effect of buffer length limit, N for the UAVRN stage and L at the BS stage, on queuing performance, we used different capacity limits on both stages of the queue while varying λ_1 at the boundary of critical λ_1 but maintaining the other parameters at the standard values. Table 7 shows the effect of N on MQL at both stages while Table 8 shows the effect of L on MQL at both stages.

Table 7 Effect of UAV-RN buffer length on MQL_{UAVRN} and MQL_{BS}

MQL_{UAVRN}				MQL_{BS}		
λ_1	Iter	Sim	$D\%$	Iter	Sim	$D\%$
$N = 3000$						
400	0.7444	0.7645	2.629169392	13.6598	13.9929	2.380492964
500	0.9979	0.9991	0.120108097	750	730.7709	2.631344516
600	1.2417	1.2217	1.637063109	1495.998	1484.7462	0.757826489
$N = 7500$						
400	0.7544	0.7644	1.308215594	13.6768	13.9764	2.14361352
500	0.9988	0.9992	0.040032026	742.83	737.2732	0.753696188
600	1.2445	1.2215	1.882930823	1496.7291	1484.7605	0.806096337
$N = 10000$						
400	0.7584	0.7645	0.797907129	13.6838	13.9606	1.982722806
500	0.999	0.9994	0.040024014	720.8843	718.8501	0.28297972
600	1.2317	1.2216	0.826784545	1495.998	1484.74	0.758247235

Table 8 Effect of BS buffer length on MQL_{UAVRN} and MQL_{BS}

MQL_{UAVRN}				MQL_{BS}		
λ_1	Iter	Sim	$D\%$	Iter	Sim	$D\%$
$L = 3000$						
400	0.7444	0.7645	2.629169392	13.6598	13.9929	2.380492964
500	0.9977	0.9987	0.100130169	1439.2315	1443.1317	0.270259464
600	1.2414	1.2214	1.637465204	2995.998	2984.6705	0.379522631
$L = 7500$						
400	0.7544	0.7644	1.308215594	13.6598	13.9703	2.202971183
500	0.9988	0.9988	0.000000000	3789.2315	3788.7124	0.065001841
600	1.2445	1.2215	1.882930823	7495.998	7484.1805	0.122119763
$L = 10000$						
400	0.7584	0.7645	0.797907129	13.6598	13.9675	2.202971183
500	0.999	0.9984	0.060096154	4582.2315	4579.2549	0.065001841
600	1.2313	1.2215	0.802292264	9995.998	9983.8058	0.122119763

For Table 7 the parameters are selected as $\lambda_1 = 500$, $\mu_1 = 2000$, $\lambda_2 = 500$, $\mu_2 = 1000$, $\theta_1 = 0.5$, $\theta_2 = 0.5$, $L = 1500$. For Table 8, the same parameters are used with the addition of $N = 1500$.

As projected, in both cases investigating the bearing of buffer length limits on mean queue length, the effect of the higher μ_1 value (maintained at 2000 packets per second) meant that the BS stage of the queue governs the stability of the system. Owing to this, the mean queue length at the UAV-RN stage is still observed to be very low in comparison to that at the BS even after the critical λ_1 has been reached, the MQL at the BS stage is at a value very close to the set buffer length limit and the system is approaching instability.

6 Limitations and future work

While we have provided discussions on the main contributions of the model and the solution approach introduced in this study, it is essential to acknowledge the limitations as well. Some of these limitations raise important questions that inspire future research endeavours, underscoring the significance of this section.

One of the issues we observed is the extreme sensitivity of the model to system instability. In the case of configurations close to unstable conditions, the discrepancy between the simulation results and the results of the analytical model is high. However, this does not tamper with the correctness of the results. It is also possible to further enhance the initial conditions used for computing the

state probabilities ($P_{i,j}$) to further expedite convergence by reducing the required number of iterations.

Considering the energy sensitivity of the application, comprehensive energy consumption models for UAV-assisted networking solutions can also be added specifically for frameworks that involve the use of UAVs solely as relay nodes and not as hovering base stations. Furthermore, concerning the queuing model, it is also possible to incorporate breakdowns and repairs of the UAV-RNs and BSs to stress-test the model.

7 Conclusion

In this study, a relaying scheme is considered for wireless connectivity during disaster recovery and its performance is evaluated using an analytical solution. The scheme under study is modelled using a two-stage tandem queuing system and used to investigate the effect of varying system parameters, particularly at the mobile relay node - arrival rates, service rates, relaying and feedback probabilities - on key performance measures, namely mean queue length, throughput and response time. In addition, with a novel augmented approach to generating the initial conditions, an iterative method is employed to provide an analytical solution for the proposed queuing system with very large queue sizes to circumvent the state explosion problem that is characteristic of the generic matrix-based solutions. The solution is, in turn, used to explore the optimum parameters under which the system would operate while maintaining its stability.

The model and analytical solution are particularly useful for identifying the critical primary UAV-RN arrival rate, λ_1 , which is the optimum primary arrival rate of packets at the UAV-RN for various relaying (θ_1) and feedback probabilities (θ_2).

The results from the proposed analytical model are presented comparatively with the results from a discrete event simulation throughout the study. The results presented for stable system analysis were with a discrepancy less than 5%, which is the confidence interval of the discrete event simulation.

The proposed iterative solution allows us to carry out performance analysis for large queue capacities. In our case, the standard size assumed in the iterative solution (1500×1500) is ten times the maximum queue size computationally permissible using matrix-based solutions (150×150). Additionally, for the standard set of parameters, the proposed iterative solution provides a significantly more efficient solution compared to the simulation program, as illustrated in Table 6. While the shortest simulation time encountered is around 239 seconds, the maximum time required by the iterative analytical solution was less than 0.48 seconds. The

approach introduced for the initial computation of state probabilities was very effective in providing early convergence.

Funding Open access funding provided by the Scientific and Technological Research Council of Türkiye (TÜBİTAK). No funding was provided for this study.

Data availability No data were created or analysed in this study. Data sharing is not applicable to this article.

Declarations

Conflict of interest The authors declare that they have no conflict of interest.

Open Access This article is licensed under a Creative Commons Attribution 4.0 International License, which permits use, sharing, adaptation, distribution and reproduction in any medium or format, as long as you give appropriate credit to the original author(s) and the source, provide a link to the Creative Commons licence, and indicate if changes were made. The images or other third party material in this article are included in the article's Creative Commons licence, unless indicated otherwise in a credit line to the material. If material is not included in the article's Creative Commons licence and your intended use is not permitted by statutory regulation or exceeds the permitted use, you will need to obtain permission directly from the copyright holder. To view a copy of this licence, visit <http://creativecommons.org/licenses/by/4.0/>.

References

1. Ever, E., Gemikonakli, E., Nguyen, H.X., Al-Turjman, F., & Yazici, A. (2020). Performance evaluation of hybrid disaster recovery framework with d2d communications. *Computer Communications*
2. Zhao, N., Lu, W., Sheng, M., Chen, Y., Tang, J., Yu, F.R., & Wong, K.-K. (February 2019). Uav-assisted emergency networks in disasters. *IEEE Wireless Communications, integrating uavs into 5G and beyond*.
3. Erdelj, M., & Natalizio, E. (2016). Uav-assisted disaster management: Applications and open issues. *IEEE Transactions on Visualization and Computer Graphics*, 19, 1–5.
4. Christy, E., et al. (2017). Optimum UAV flying path for device-to-device communications in disaster area, 318–322
5. Chen, Y., et al. (2018). Multiple UAVS as relays: Multi-hop single link versus multiple dual-hop links. *IEEE Transactions on Wireless Communications*, 17(9), 6348–6359.
6. Alzahrani, B., Oubbati, O. S., Barnawi, A., Atiquzzaman, M., & Alghazzawi, D. (2020). UAV assistance paradigm: State-of-the-art in applications and challenges. *Journal of Network and Computer Applications*. <https://doi.org/10.1016/j.jnca.2020.102706>
7. Jiang, F., & Phillips, C. (2020). High throughput data relay in uav wireless networks. *Future Internet*, 12, 193. <https://doi.org/10.3390/fi12110193>
8. He, Y., Zhai, D., Wang, D., Tang, X., & Zhang, R. (2020). A relay selection protocol for UAV-assisted vanets. *Applied Sciences*. <https://doi.org/10.3390/app10238762>
9. Mozaffari, M., Saad, W., Bennis, M., & Debbah, M. (2016). Efficient deployment of multiple unmanned aerial vehicles for optimal wireless coverage. *IEEE Communications Letters*. <https://doi.org/10.1109/JIOT.2021.3051361>

10. Bisnik, N., & Alhussein, A. (2009). Queuing network models for delay analysis of multihop wireless ad hoc networks. *Ad Hoc Networks*, 7, 79–97. <https://doi.org/10.1016/j.adhoc.2007.12.001>
11. Yaqoob, M., Ever, E., & Gemikonakli, O. (2020). Modelling heterogeneous future wireless cellular networks: An analytical study for interaction of 5g femtocells and macro-cells. *Future Generation Computer Systems* 114, 82–95. <https://doi.org/10.1016/j.future.2020.07.049>. Computer Engineering, Middle East Technical University, Northern Cyprus Campus, 99738, Mersin 10, Guzelyurt, Turkey and Computer Design Engineering, Middlesex University, London, UK (*resp.*)
12. Ever, E., Gemikonakli, O., & Kocyigit, A. (2007). Approximate solution for two stage open networks with markov-modulated queues minimizing the state space explosion problem. *Journal of Computational and Applied Mathematics*, 223, 519–533. <https://doi.org/10.1016/j.cam.2008.02.009>
13. Jiang, X., Sheng, M., Zhao, N., Xing, C., Lu, W., & Wang, X. (2021). Green UAV communications for 6g: A survey. *Chinese Journal of Aeronautics*. <https://doi.org/10.1016/j.cja.2021.04.025>
14. Tuna, G., Mumcu, T., & Gulez, K. (2012). Design strategies of unmanned aerial vehicle-aided communication for disaster recovery, pp. 115–119. <https://doi.org/10.1109/HONET.2012.6421446>
15. Merwaday, A., & Guvenc, I. (2015). Uav assisted heterogeneous networks for public safety communications. In: 2015 IEEE Wireless Communications and Networking Conference Workshops (WCNCW), pp. 329–334. <https://doi.org/10.1109/WCNCW.2015.7122576>
16. Ueyama, J., Freitas, H., Faical, B., Filho, G., Fini, P., Pessin, G., Gomes, P., & Villas, L. (2014). Exploiting the use of unmanned aerial vehicles to provide resilience in wireless sensor networks. *IEEE Communications Magazine*. <https://doi.org/10.1109/MCOM.2014.6979956>
17. Robinson, W. H., & Lauf, A. P. (2013). Aerial manets: Developing a resilient and efficient platform for search and rescue applications. *Journal of Communication*, 8, 216–224.
18. Bupe, P., Haddad, R., & Rios-Gutierrez, F. (2015). Relief and emergency communication network based on an autonomous decentralized uav clustering network. In: SoutheastCon 2015, pp. 1–8. <https://doi.org/10.1109/SECON.2015.7133027>
19. Mukherjee, A., Dey, N., Kumar, R., Panigrahi, B. K., Hasanien, A. E., & Tavares, J. M. R. S. (2019). Delay Tolerant Network assisted flying Ad-Hoc network scenario: modeling and analytical perspective. Springer. <https://doi.org/10.1007/s11276-019-01987-8>
20. Felice, M.D., Trotta, A., Bedogni, L., Chowdhury, K.R., & Bononi, L. (2014). Self-organizing aerial mesh networks for emergency communication. In: 2014 IEEE 25th Annual International Symposium on Personal, Indoor, and Mobile Radio Communication (PIMRC), 1631–1636.
21. Vamvakas, P., Tsiropoulou, E.E., & Papavassiliou, S. (2019). On the prospect of uav-assisted communications paradigm in public safety networks. In: IEEE INFOCOM 2019 - IEEE Conference on Computer Communications Workshops (INFOCOM WKSHPS), pp. 762–767. <https://doi.org/10.1109/INFOCOMW.2019.8845131>
22. Zeng, Y., Zhang, R., & Lim, T.J. (2016). Wireless communications with unmanned aerial vehicles: Opportunities and challenges
23. Mozaffari, M., Saad, W., Bennis, M., Nam, Y.-H., & Debbah, M. (2019). A tutorial on UAVS for wireless networks: Applications, challenges, and open problems
24. Zhang, S., & Liu, J. (2018). Analysis and optimization of multiple unmanned aerial vehicle-assisted communications in post-disaster areas. *IEEE Transactions on Vehicular Technology*, 67(12), 12049–12060. <https://doi.org/10.1109/TVT.2018.2871614>
25. TechTarget: Network Packet. <https://www.techtarget.com/searchnetworking/definition/packet#:~:text=Typically%2C%20a%20packet%20holds%201%2C000,internet%20address%20of%20the%20destination>. Accessed: 2022-04-23 (July 2021)
26. LIFEWIRE: 5G: Everything You Need to Know. <https://www.lifewire.com/5g-wireless-4155905#:~:text=5G%20Supports%20Lots%20of%20Devices,internet%20at%20the%20same%20time>. Accessed: 2022-06-19 (June 18, 2021)
27. Noura, M., & Nordin, R. (2016). A survey on interference management for device-to-device (d2d) communication and its challenges in 5g networks. *Journal of Network and Computer Applications*, 71, 130–150. <https://doi.org/10.1016/j.jnca.2016.04.021>
28. Trabelsi, N., Chaari Fourati, L., & Chen, C. S. (2024). Interference management in 5g and beyond networks: A comprehensive survey. *Computer Networks*, 239, 110159. <https://doi.org/10.1016/j.comnet.2023.110159>
29. Chu, Z., Nguyen, H. X., Le, T. A., Karamanoglu, M., Ever, E., & Yazici, A. (2018). Secure wireless powered and cooperative jamming d2d communications. *IEEE Transactions on Green Communications and Networking*, 2(1), 1–13. <https://doi.org/10.1109/TGCN.2017.2763826>
30. Al-Turjman, F., Ever, E., & Zahmatkesh, H. (2017). Green femtocells in the IoT era: Traffic modeling and challenges-an overview. *IEEE Network*, 31(6), 48–55.
31. Kirsal, Y., Ever, E., Kocyigit, A., Gemikonakli, O., & Mapp, G. (2015). Modelling and analysis of vertical handover in highly mobile environments. *Journal of Supercomputing*. <https://doi.org/10.1007/s11227-015-1528-3>
32. Kirsal, Y., Ever, E., Kocyigit, A., Gemikonakli, O., & Mapp, G. (2014). A generic analytical modelling approach for performance evaluation of the handover schemes in heterogeneous environments. *Wireless Personal Communications*, 79, 1247–1276. <https://doi.org/10.1007/s11277-014-1929-2>
33. Ciardo, G., Blakemore, A., Chimento Jr, P.F., Muppala, J.K., & Trivedi, K.S. (1993). Automated generation and analysis of markov reward models using stochastic reward nets. In: Linear Algebra, Markov Chains, and Queueing Models, pp. 145–191. Springer
34. Donmez, B., Nehme, C., & Cummings, M. L. (2010). Modeling workload impact in multiple unmanned vehicle supervisory control. *IEEE Transactions on Systems, Man, and Cybernetics-Part A: Systems and Humans*, 40, 1180–1190.
35. Banks, J., Carson, J.S.I., Nelson, B.L., & Nicol, D.M. (2005). Discrete-event system simulation, 4th Edn. Prentice Hall - Pearson education
36. El-atty, S. M. A., & Gharseldien, Z. M. (2017). Performance analysis of an advanced heterogeneous mobile network architecture with multiple small cell layers. *Wireless Networks*, 23, 1169–1190. <https://doi.org/10.1007/s11276-016-1218-y>
37. Chandhar, P., & Larsson, E. G. (2019). Massive mimo for connectivity with drones: Case studies and future directions. *IEEE*. <https://doi.org/10.1109/ACCESS.2019.2928764>
38. Intel: Specifications for the Intel@Aero Ready to Fly Drone. <https://www.intel.com/content/www/us/en/support/ARTICLES/000023272/drones/development-drones.html>. Accessed: 2022-09-1 (February 2019)
39. Chan, S. C. F., Chan, K. M., Liu, K., & Lee, J. Y. B. (2014). On queue length and link buffer size estimation in 3g/4g mobile data networks. *IEEE Transactions on Mobile Computing*, 13, 1298–1311. <https://doi.org/10.1109/TMC.2013.127>

Publisher's Note Springer Nature remains neutral with regard to jurisdictional claims in published maps and institutional affiliations.



Eugene Casmin received his B.Sc. and M.Sc. Degrees in Computer Engineering from Middle East Technical University, Northern Cyprus Campus. He is currently pursuing his Ph.D. in Electrical and Computer Engineering at Nova School of Science and Technology (NOVA FCT) in Lisbon, Portugal, and is attached to the Institute of Telecommunications as a Research Fellow.

2013. He is a full Professor at the Middle East Technical University Northern Cyprus Campus. His current research interests include the Internet of Things, computer networks, wireless sensor networks, wireless multimedia sensor networks, artificial intelligence (machine learning/deep learning) applications, wireless communication systems, cloud computing, and performance/reliability modelling. He serves on various boards and program committees.



Enver Ever received an M.Sc. degree in computer networks and a Ph.D. in performance evaluation of computer networks and communication systems from Middlesex University, London, in 2004 and 2008, respectively. He was a Post-Doctoral Research Associate with Bradford University for one year. He was a Lecturer/Senior Lecturer with the Computer and Communications Engineering Department at Middlesex University from 2008 to